frontiers in Energy Research

ORIGINAL RESEARCH
published: 21 May 2021
doi: 10.3389/fenrg.2021.647878

Supercapacitor with Carbon/MoS_2 Composites

*Maciej Tobis, Sylwia Sroka and Elżbieta Frąckowiak**

Institute of Chemistry and Technical Electrochemistry, Poznan University of Technology, Poznan, Poland

Transition metal dichalcogenides (TMDs) with a two-dimensional character are promising electrode materials for an electrochemical capacitor (EC) owing to their unique crystallographic structure, available specific surface area, and large variety of compounds. TMDs combine the capacitive and faradaic contribution in the electrochemical response. However, due to the fact that the TMDs have a strong catalytic effect of promoting hydrogen and oxygen evolution reaction (HER and OER), their usage in aqueous ECs is questioned. Our study shows a hydrothermal L-cysteine–assisted synthesis of two composites based on different carbon materials—multiwalled carbon nanotubes (NTs) and carbon black (Black Pearl-BP2000)—on which MoS_2 nanolayers were deposited. The samples were subjected to physicochemical characterization such as X-ray diffraction and Raman spectroscopy which proved that the expected materials were obtained. Scanning electron microscopy coupled with electron dispersive spectroscopy (SEM/EDS) as well as transmission electron microscopy images confirmed vertical position of few-layered MoS_2 structures deposited on the carbon supports. The synthetized samples were employed as electrode materials in symmetric ECs, and their electrochemical performance was evaluated and compared to their pure carbon supports. Among the composites, NTs/MoS_2 demonstrated the best electrochemical metrics considering the conductivity and capacitance (150 Fg^{-1}), whereas BP2000/MoS_2 reached 110 Fg^{-1} at a current load of 0.2 Ag^{-1}. The composites were also employed in a two-electrode cell equipped with an additional reference electrode to monitor the potential range of both electrodes during voltage extension. It has been shown that the active edge sites of MoS_2 catalyze the hydrogen evolution, and this limits the EC operational voltage below 1 V. Additional tests with linear sweep voltammetry allowed to determine the operational working voltage for the cells with all materials. It has been proven that the MoS_2/carbon composites possess limited operating voltage, that is, comparable to a pure MoS_2 material.

Keywords: molybdenum disulfide, transition metal dichalcogenide, 2D materials, carbon nanotubes, carbon black, electrochemical capacitors, neutral electrolyte

OPEN ACCESS

Edited by:
Ana Karina Cuentas Gallegos, National Autonomous University of Mexico, Mexico

Reviewed by:
Yong Zhang, Hefei University of Technology, China
Jeng-Yu Lin, Tatung University, Taiwan

****Correspondence:***
Elżbieta Frąckowiak
elzbieta.frackowiak@put.poznan.pl

Specialty section:
This article was submitted to Electrochemical Energy Conversion and Storage, a section of the journal Frontiers in Energy Research

Received: *30 December 2020*
Accepted: *23 April 2021*
Published: *21 May 2021*

Citation:
Tobis M, Sroka S and Frąckowiak E (2021) Supercapacitor with Carbon/MoS_2 Composites. Front. Energy Res. 9:647878. doi: 10.3389/fenrg.2021.647878

INTRODUCTION

The industry is constantly facing issues on advanced and more efficient energy storage systems for intermittent renewable energy harvesting that can successfully inhibit the overexploitation of natural reserves of fossil fuels. For this reason, a booming interest in the area of research and development of energy storage devices has been noted. Electrochemical capacitors (ECs) in particular, owing to their remarkable features such as superior cyclability and high-power density, can be successfully employed in this field (Sharma and Bhatti, 2010; Chen, 2016; González et al., 2016). However, in order to compete with modern batteries, the research aim is largely focused on increasing EC energy density while retaining their fast charge/discharge rate. The performance of such storage devices can be effectively improved through extension of voltage window or an increase of specific capacitance, as shown in the following equation (Simon and Gogotsi, 2008):

$$E = \frac{1}{2} C \cdot V^2$$

where E represents energy density, C capacitance, and V the operating voltage. As the energy in ECs is stored mainly through adsorption of ions at electrode/electrolyte interface, one of the major requirements for the electrode materials is developed specific surface area (SSA) and high conductivity. Electrode materials based on carbons have been already well known to possess those characteristic features (Frackowiak and Béguin, 2001; Pandolfo and Hollenkamp, 2006; Cherusseri et al., 2016; Ratajczak et al., 2019). Although, due to limitations related to a nonuniform distribution of pores and their availability for ions, they usually offer capacitance ca. 100 Fg^{-1} (Fic et al., 2012). For this reason, a regained interest in the field of electrode material development such as ones based on transition metal dichalcogenides (TMDs) has been observed. These two-dimensional inorganic materials, including MoS_2, WS_2, VS_2, or $MoSe_2$ (Acerce et al., 2015; Balasingam et al., 2015; Chen et al., 2019; Xu et al., 2020), can possess both "faradaic" and "non-faradaic" behaviors, very thin structure (which in turn leads to short transport length for electrons and ion migration), high conductivity, and large surface tunability (Coogan and Gun'ko, 2021; Lukatskaya et al., 2016; Bissett et al., 2016; Choi et al., 2017; Zhang and Huang, 2017). Thanks to these qualities, TMDs can be effectively employed as electrode materials for ECs. MoS_2, in particular, has been extensively studied in capacitor applications over the past few years. Layered MoS_2 consists of a single Mo atom sandwiched between two S atoms, with weak Van der Waals interactions stacking them together. One way in which the electronic conductivity of the composite can be noticeably improved is the incorporation of conducting materials, such as carbon blacks or carbon nanotubes (CNTs) (Yang et al., 2017; Lin et al., 2019; Sun et al., 2019). However, when paired with an aqueous electrolyte, the EC system is characterized by a narrow voltage window due to electrolysis of water, which, in turn, affects its energy density. In electrochemical systems, this process is governed by oxygen evolution reaction (OER) and hydrogen evolution reaction (HER). However, aqueous electrolytes have superior advantage in terms of safety, cost, feasibility of use, and eco-friendliness, as compared to organic electrolytes (Zhong et al., 2015). A lot of research has been devoted to TMD composites as EC materials and very high capacitance values exceeding even 400 Fg^{-1} have been reported, but most of these studies are performed only in a three-electrode system with an excess of electrolyte, the mass of electrode is often below 1mg, and calculations are not always correct. Hence, apart from the fundamental significance, practical application of some studies is meaningless. From our point of view, only investigation in a two-electrode system resembles a real capacitor performance. Estimation of safe operating voltage of capacitor with TMD-based electrodes is crucial. Unfortunately, the reason of voltage limitation was not studied in detail. Electrochemical reactions associated with activity of MoS_2 result in its inherent limited potential window. Nasir et al. have reported an electrochemical window of MoS_2 where both anodic and cathodic regions were investigated (Nasir et al., 2015). At the anodic potentials, oxidation of Mo^{4+} to Mo^{6+} occurs, while at the cathodic potentials, the reduction of H_3O^+ present in the solution results in electrocatalytic HER at the surface of MoS_2 (Nasir et al., 2015; Sangeetha and Selvakumar, 2018; Tseng and Lee, 2020; Yuan et al., 2020). Hence, even if interconnected network is created, such as in MoS_2/carbon-based materials, TMD presence can lead to enhanced HER activity due to its morphology and much faster movement of electrons (Sangeetha et al., 2020; Rendón-Patiño et al., 2020). All the parameters mentioned have a great impact on the potential window of MoS_2-based materials and have to be considered carefully.

In this study, the MoS_2 composites with 7 wt% amount of BP2000 or NTs were prepared with the use of hydrothermal process utilizing L-cysteine which acted as an effective and nontoxic source of sulfur in the reaction (Huang et al., 2013; Park et al., 2013; Huang et al., 2014). Synthetized composites and sole materials were physicochemically characterized, prepared in the form of electrodes, and further studied electrochemically in two-electrode and two-electrode with reference cells with a special attention to voltage frontiers.

EXPERIMENTAL

Material Synthesis

Layered MoS_2 was obtained during a hydrothermal reaction. 1.6 g of L-cysteine (Sigma Aldrich, 97%) and 0.6 g of $Na_2MoO_4{\cdot}2H_2O$ (Sigma Aldrich, ≥ 99%) were mixed in 80 ml of DI water. Then, the pH of the solution was adjusted to 6 with the use of 5% HCl which turned the solution from colorless to scarlet orange. The mixture of the precursors was then transferred into a stainless steel autoclave (Parr® 5500 Series compact reactor) for 24 h at 210°C. After the reaction, the solution was filtered and washed several times with DI water and isopropanol. Black powder was collected and dried at 70°C for 12 h. The composites of NTs/MoS_2 and BP2000/MoS_2 were synthetized accordingly but with the use of NTs (IoLiTec nanomaterials, outer diameter: 20–40 nm, length: 5–15 μm, and > 95% purity) and BP2000 (Cabot). 0.035 g of the NTs and BP2000 were sonicated (Hielsher UP50H) for 30 min and then mixed with the solution of precursors. The resulting solution was treated as prior, and composite sample was collected and dried. The process of

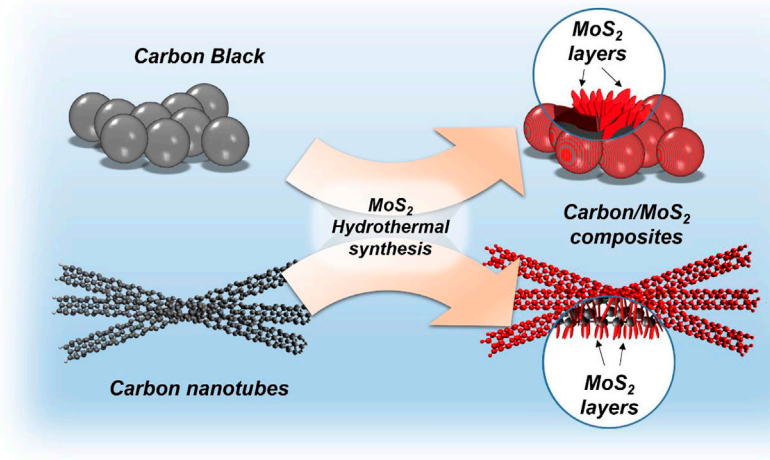

FIGURE 1 | Simplified process of carbon/MoS_2 synthesis.

synthesis (**Figure 1**) can be presented by the following equations (Chang and Chen, 2011).

$$HSCH_2CHNH_2COOH + H_2O \rightarrow CH_3COCOOH + NH_3 + H_2S$$

$$4MoO_4^{2-} + 9H_2S + 6CH_3COCOOH \rightarrow 4MoS_2 + SO_4^{2-} + 6CH_3COCOO^- + 12H_2.$$

Materials Characterization

Raman scattering spectroscopy was performed using a Thermo Scientific DXR Raman Microscope with a laser emitting at $\lambda = 532$ nm and power of 5 mW. The total exposure time was 60 s, carried out in 3 scans series, and each lasting 20 s. The measurements were repeated at least 3 times for each sample at different locations to ensure uniformity throughout.

Scanning electron microscope (SEM) Tescan Vega 5135 coupled with the PTG Avalon X-ray microanalyzer adapter for the evaluation of the energy dispersive spectroscopy (EDS) was employed to study the texture morphology and atomic content on the surface of the material at different magnifications.

Additional structural and morphological studies were performed by transmission electron microscopy (TEM) FEI Titan G2 80-300 equipped with an energy dispersive X-ray spectrometer (Hillsboro, OR, United Sates).

In order to confirm crystallographic structures, the samples were investigated by X-ray diffraction (XRD) technique employing BRUKER D8 Advanced, equipped with Johansson monochromator using Cu Kα radiation (Cu Kα, λ = 1.5406 Å) and silicon strip detector Lynx Eye. The minimum measurement angle was 0.6 of 2θ degree.

Electrode Preparation and Electrochemical Tests

The electrodes were prepared from 90wt% of an active material, 5 wt% of a conducting agent (C-NERGY™ Super C65, Imerys), and 5 wt% of polytetrafluoroethylene binder (60% dispersion in water

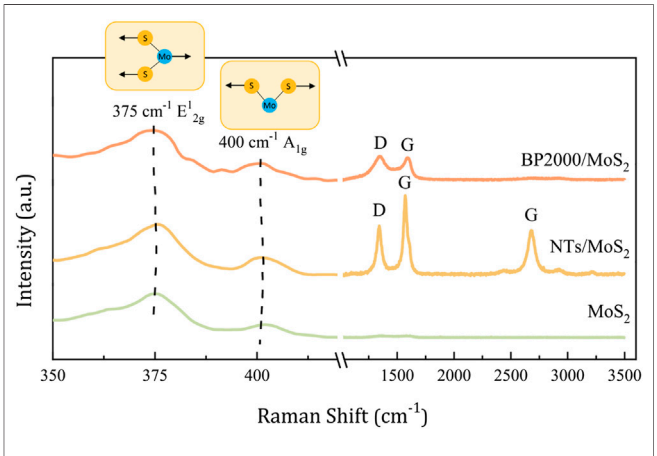

FIGURE 2 | Raman spectra of BP2000/MoS_2, NTs/MoS_2, and MoS_2.

PTFE, Sigma Aldrich). The materials were weighed and mixed with isopropanol and sonicated for 30 min. After isopropanol was evaporated and dough-like consistency of the material was obtained, it was then transferred in-between two sheets of plastic foil, rolled, and passed through a hot roller in order to obtain a uniform thickness of about 200 μm. Then, it was cut into disc electrodes of a 10mm diameter and dried at 70°C for 24 h in an oven.

Symmetric electrochemical capacitors with stainless steel 316L current collectors were assembled with two electrodes of equal mass (ca. 10 mg). They were soaked with an appropriate amount of electrolyte (1M Li_2SO_4), then separated with a glass microfiber membrane (GF/A, Whatman™, thickness of 260 μm and disc diameter 12 mm), and mounted under normal atmosphere using Teflon Swagelok® tube fitting. Hg/Hg_2SO_4 served as a reference electrode to monitor performance of both electrodes. The voltammetry response of each electrode was determined according to the previous investigations (Slesinski and Frackowiak, 2018). The specific capacitance per one electrode

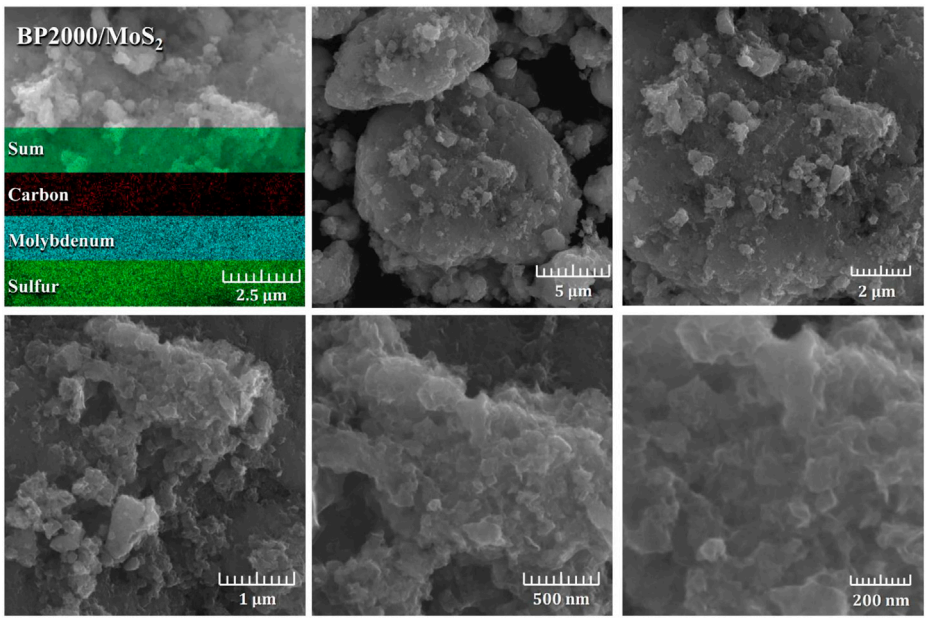

FIGURE 3 | EDS and SEM images of BP2000/MoS_2 at different magnifications.

was calculated according to a very well-known methodology (Laheäär et al., 2015). Taking into account the information gathered from all electrochemical measurements and calculations, a successful comparison between each material was completed.

RESULTS AND DISCUSSION

Material Characterization

Raman spectroscopy allowed to obtain information regarding a chemical composition of MoS_2 and its composites with BP2000 and NTs. **Figure 2** shows Raman spectrum of BP2000/MoS_2, NTs/MoS_2, and MoS_2 composites. Spectrum contains distinctive G and D band peaks at 1,604 and 1,345 cm^{-1}, respectively, with a loss of intensity for both peaks. Raman spectrum of NTs/MoS_2 composite showed three distinctive features: two sharp peaks at ~1,575 and ~1,345 cm^{-1} belonging to G (graphite in plane mode due to stretching vibrations of C–C bond) and D (disorder) band, respectively. D band of BP2000 is widened due to disordered structure and amorphous nature of the BP2000 instead of less defects than the CNTs. G′ second order harmonic is visible at ~2,685 cm^{-1} (Zdrojek et al., 2004). In both samples, the G band can be further divided into G1 and G2 bands at 1,572 and 1,608 cm^{-1}, respectively. These bands are related to lattice vibration of sp^2 bond carbon materials, as reported in other works (Rao et al., 1997; Duesberg et al., 2000). Raman spectrum bands at ~ 375 cm^{-1} can be assigned to an in-plane E_{2g} mode where sulfur atoms vibrate in one direction, whereas molybdenum in another direction, with a literature value of 400 cm^{-1} (Conley et al., 2013).

Figure 3 shows SEM and EDS images of BP2000/MoS_2. Carbon blacks are known to be created from the spherical particles which connected together form a complex micro- and mesoporous bead-like structure. SEM images revealed that the composite, comparable to NTs/MoS_2 (**Figure 4**), has remained in the original shape of BP2000 and NTs, accordingly. Higher magnifications show that the surface of the composites is covered by the MoS_2 nanolayers which form accessible structure favorable for transportation and diffusion of ions during adsorption/desorption. EDS mappings (**Figures 3** and **4**) show the elemental distribution on the surface of the composite. Presence of Mo, S, and C atoms is confirmed in both cases, that is, BP2000/MoS_2 and NTs/MoS_2. A low amount of carbon detected suggests tight and homogenous coverage of carbon supports by MoS_2 layers. During the synthesis process, MoS_2 layers are formed and deposited on the surface of the NTs favorably at the defect sites. The layers are directed perpendicularly or horizontally to the NTs surface. Generally, "bottom-up" methods such as hydrothermal synthesis are characterized by low controllability of the process, unlike chemical vapor deposition (CVD) (Gao et al., 2016). Therefore, it is most likely that the composite possesses randomly positioned layers with a major perpendicular orientation (inset of **Figures 3** and **4**). Such unique structure possesses many adsorption sites for ions created by deposited MoS_2 layers and quick diffusion routes originating mostly from NTs and BP2000.

Transmission electron microscopy (TEM) was conducted to determine the microstructure and crystallinity of the composites. TEM images in **Figures 5A,E** showed consistency with the SEM/EDX results in **Figure 4**. High

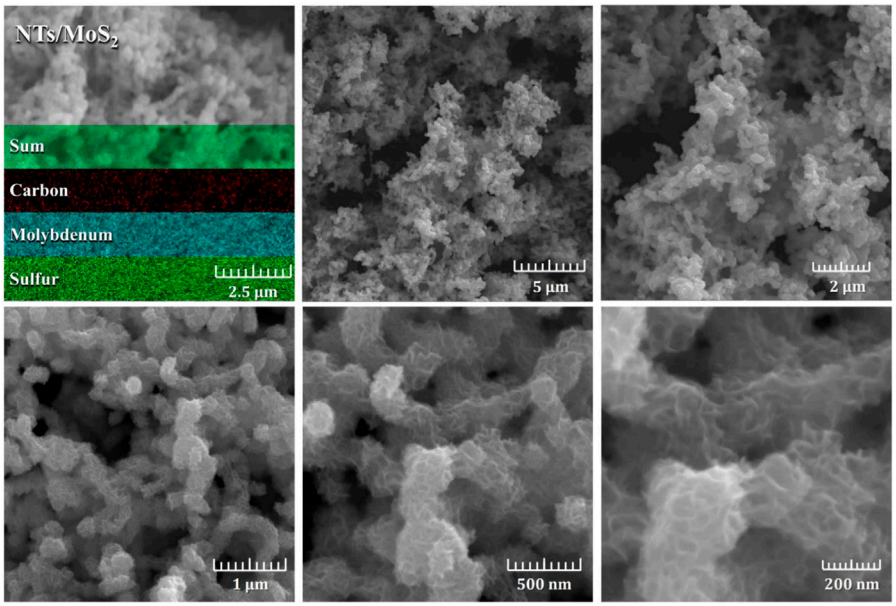

FIGURE 4 | EDS and SEM images of NTs/MoS_2 at different magnifications.

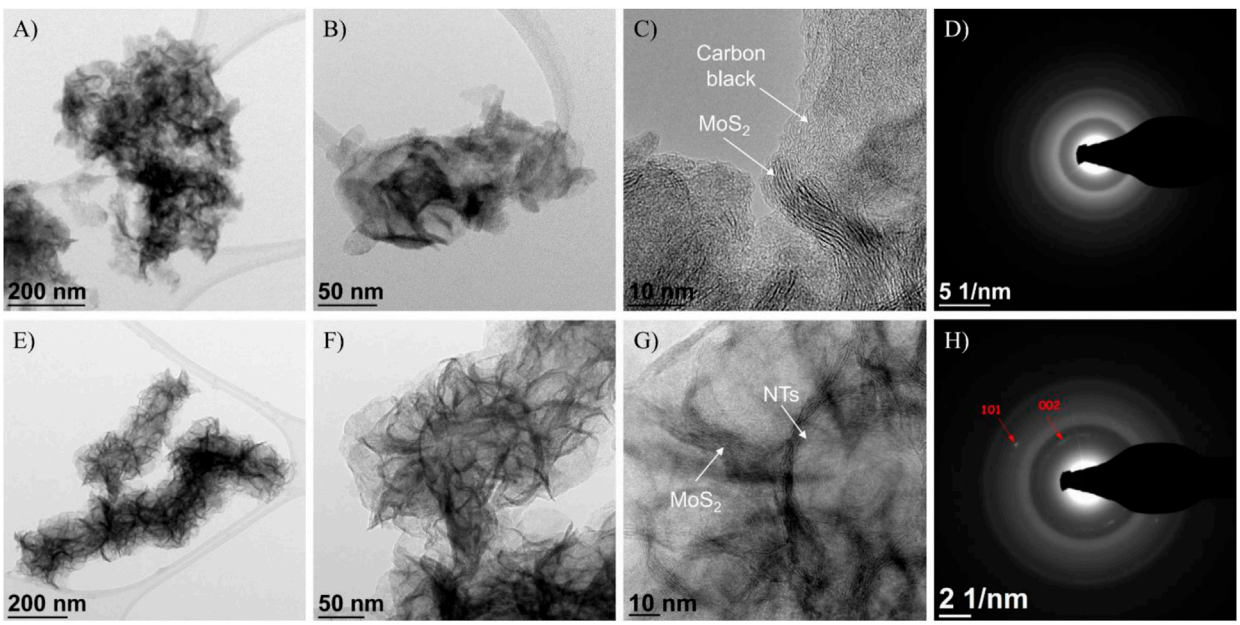

FIGURE 5 | TEM and SAED images of BP2000/MoS_2—**(A)–(D)** and NTs/MoS_2—**(E)–(H)**.

magnifications of BP2000/MoS_2 (**Figure 5C**) show two significantly different sections in the image. Wide disordered area can be attributed to carbon black, while black lines can be considered as MoS_2 edged layers. Images show that the MoS_2 layers are predominantly grown in the vertical direction to the carbon support. Additionally, MoS_2 present in the form of few layers stacks is strongly linked to carbon support. Sample NTs/MoS_2 showed comparable stacking, although it seems that the MoS_2 are much better distributed on the NTs surface. It may origin from the mesoporous character of the NTs. The number of individual layers of MoS_2 appears to be lower which can also be attributed to the texture of NTs. In both cases, selected area electron diffraction (SAED—**Figures 5D,H**) patterns showed weak diffraction rings indicating low crystallization of MoS_2.

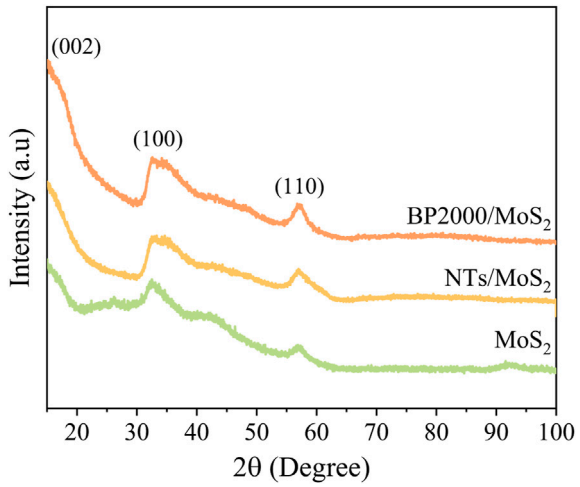

FIGURE 6 | X-ray diffractograms for different materials.

For the NTs/MoS_2 sample, it was possible to differentiate two weak diffraction rings, that is, 002 and 101 attributed to NTs. The XRD method allowed to investigate the crystallographic structure of the samples. **Figure 6** shows diffractogram patterns registered for MoS_2, $BP2000/MoS_2$, and NTs/MoS_2. Each sample exhibited peaks at 17°, 33°, and 58° indicating (002), (100), and (110) planes of MoS_2, respectively (JCPDS card number 37-1492). Low intensity of the peaks is related to the disordered and layered, differently oriented structure of the MoS_2 on the carbon supports.

Electrochemical Measurements

After physicochemical characterization, the composite materials and pure components were further investigated in the capacitor cells to evaluate the electrochemical properties. The fundamental electrochemical measurement consisted of electrochemical impedance spectroscopy (EIS) with a frequency between 100 kHz–10 mHz, followed by cyclic voltammetry (CV) from 0 to 0.8 V with varying scan rates 1, 2, 5, 10, 20, 50, 100, and 200 mVs^{-1}, galvanostatic charge/discharge at a current densities of 0.2, 0.5, 1, and 2 Ag^{-1}, and subsequent EIS measurement with the same parameters. Next, the two-electrode cell equipped with a reference electrode was subjected to a gradual CV extension of the voltage window starting from 0.6 to 1.5 V with increments of 0.1 V at a constant scan rate of 2 mVs^{-1} and galvanostatic measurements with a constant current density of 0.2 Ag^{-1}, finishing up by the EIS measurement. General comparison of capacitor metrics between each sample is shown in **Figure 7**. Additionally, the detailed electrochemical characterization including effect of scan rates and different current density applied was placed in **Supplementary Figures S1 and S2**.

A perfectly rectangular shape of the cyclic voltammetry profiles for the EC cells with carbonaceous materials is not a surprise in the low voltage ranges. Such materials are already known to be ideal capacitor materials with high conductivity. MoS_2 itself demonstrated higher capacitance than both carbons owing to the dual mechanism, that is, capacitive charge/discharge but also possible redox phenomena (lithium insertion and various oxidation state of Mo). However, the CV characteristics of MoS_2 and its composite derivatives exhibited slightly sloping shape that indicates higher intrinsic resistance of the TMD material. Both

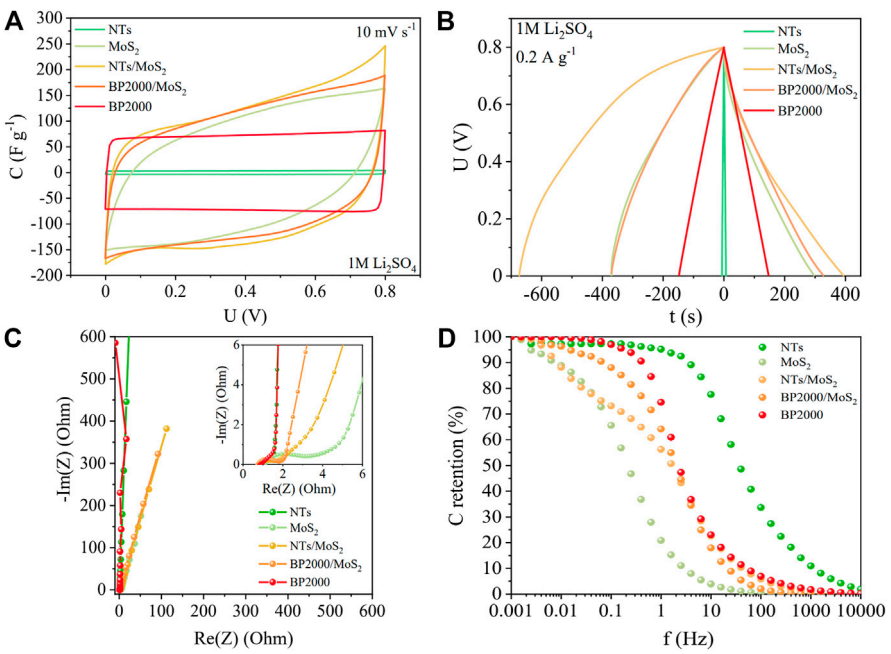

FIGURE 7 | Electrochemical performance of pure BP2000, NTs, MoS_2, and their MoS_2 composite materials. **(A)** Cyclic voltammograms, **(B)** galvanostatic charge/discharge, **(C)** electrochemical impedance spectroscopy, and **(D)** capacitance retention vs. frequency.

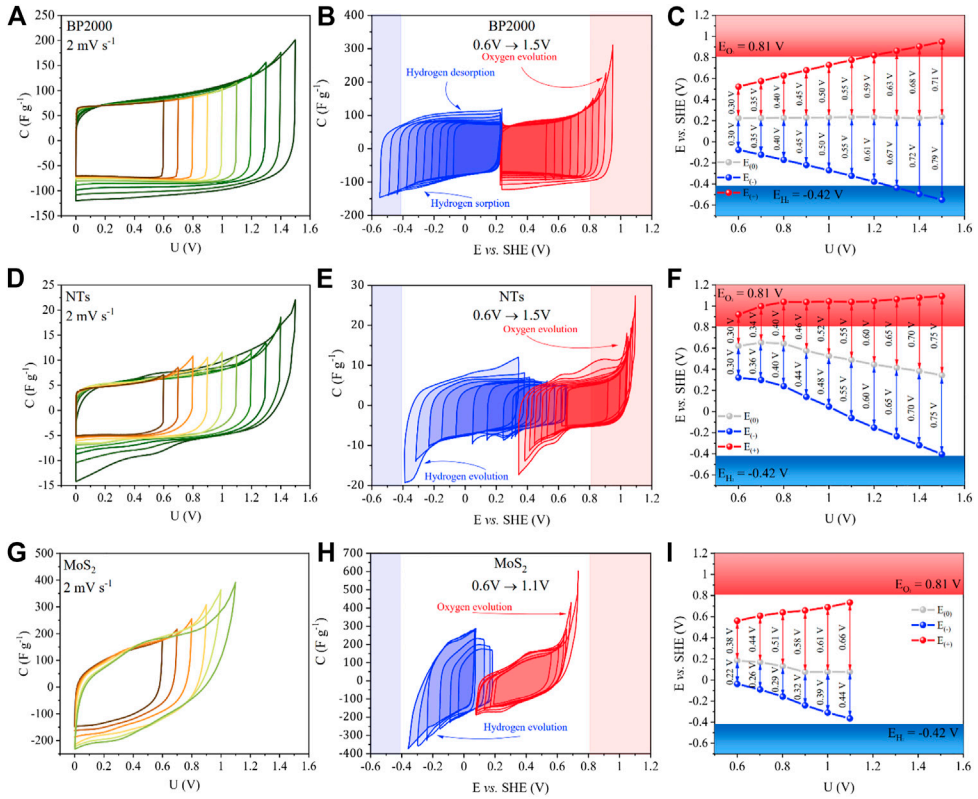

FIGURE 8 | Electrochemical characterization of symmetric EC cells. Cyclic voltammograms of gradual voltage extensions for BP2000, NTs, and MoS_2—**(A), (D),** and **(G)**. Individual cyclic voltammograms for (+) and (–) electrodes—**(B), (E),** and **(H)**. Operational potentials for both electrodes at each voltage—**(C), (F), and (I).**

EC cells with composites showed significantly higher capacitance than maternal materials. Nevertheless, the NTs/MoS_2 composite exhibited definitely better behavior than BP2000/MoS_2. **Figure 7C** presents a Nyquist plot for composites and precursor materials. Carbons in comparison to MoS_2 and its composites possessed significantly smaller intrinsic resistance. Carbon blacks and nanotubes are known to possess very high conductivity which reflects low equivalent series resistance (ESR) values (0.82 and 0.74 Ω, respectively). Fast capacitive charging of these carbons is proven by the parallel direction of line to the y-axis with equivalent distributed resistance (EDR) of 1.65 and 1.58 Ω. Oppositely, MoS_2 alone as a semiconductor possesses lower conductivity with ESR of 1.1 Ω with a distinct semicircle exhibiting EDR of 4.85 Ω. At low frequencies, MoS_2 line showed high slope reflecting diffusion effects. Such discrepancy between the values obtained from MoS_2 and carbons can be explained by the lower conductivity and high charge transfer resistance of MoS_2. Cells constructed with BP2000/MoS_2 and NTs/MoS_2 exhibited intermediate values of ESR to the parental materials (0.78 and 0.80 Ω, respectively). Additionally, slope character of the MoS_2 composites with EDR of (2.05 and 3.32 Ω, adequately) indicates diffusion effects of faradaic processes. To explain the charge propagation of the composites, the capacitance retention vs. frequency chart has been prepared (**Figure 7D**). It can be observed that the carbon black and nanotubes were able to hold their maximum capacitance up to 1 and 10 Hz, respectively. At 1 Hz, MoS_2 was able to retain only 20% of the initial capacitance which originates from its low conductivity and high charge transfer resistance. Composites prepared with BP2000 and NTs exhibited intermediate charge transfer properties as they were able to hold around 65% of the initial capacitance. It can be observed that such moderate addition of carbons (~7 wt%) to the composite has improved the overall performance of the cell. Different loadings of carbon supports in the composite mass have been studied separately (**Supplementary Figure S3**). It has been proven that 7 wt% of carbon support was an optimal amount. The morphology of both carbon supports is different; hence, the process of MoS_2 layers formation and deposition is dissimilar.

Taking into account the main goal of our research, we focused on the possibility of voltage extension and elucidation of electrochemical behavior of (+) and (–) electrode, separately. Hence, the further electrochemical performance of the samples was studied in a two-electrode cell with an additionally positioned Hg/Hg_2SO_4 reference electrode. At the beginning, operational voltage windows of the cells containing pure materials, that is, BP2000, NTs, and MoS_2 were studied. **Figure 8A** displays performance of the full cell containing BP2000 as an electrode material, whereas **Figures 8B,C** indicate performance of single electrodes. Cell with BP2000 showed steady window potential extension at both electrodes with stable rest potential. This carbon black is a micro- and mesoporous material with

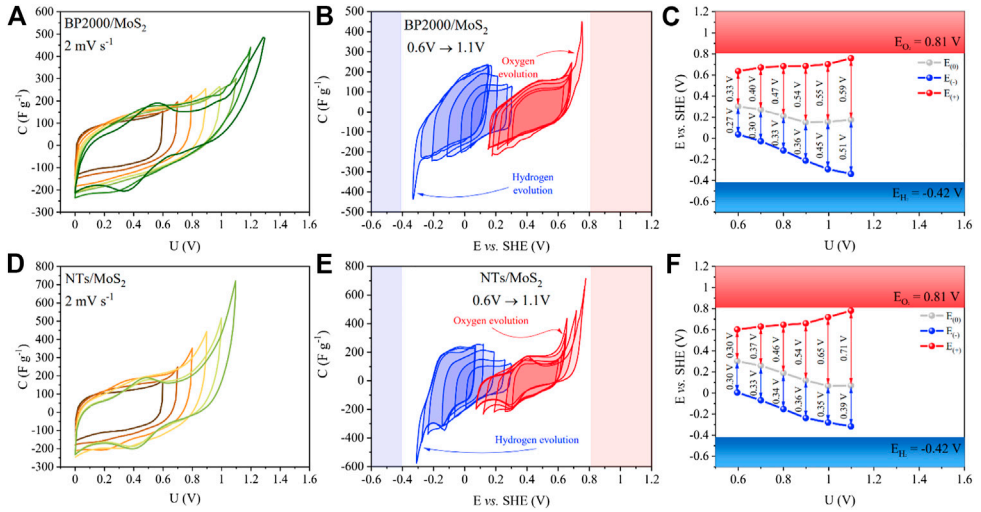

FIGURE 9 | Electrochemical characterization of symmetric EC cells based on MoS_2 composites. Cyclic voltammograms during gradual voltage extension—**(A)** and **(D)**. Individual cyclic voltammograms for (+) and (–) electrodes—**(B)** and **(E)**. Operational potentials for both electrodes at each voltage—**(C) and (F)**.

developed surface area (1540 m^2g^{-1}). Due to such unique morphology, it possesses a smaller amount of sharp edges on which the electrolyte decomposition phenomena can occur, meaning that the material can withstand higher operational voltages. Contrary, for the cell with NTs (**Figures 8D–F**) at the low voltages (0.6–0.8 V), rest potentials of both electrodes remain stable. The maximum positive and negative potential values are gradually and equally extended. Beginning from 0.9 V, the rest potential is being shifted toward more negative values. The maximum positive potential remained more or less unchanged during the tests, and it was placed within the range of oxygen evolution. NTs possess essentially mesoporous structure (90 m^2g^{-1}) which excludes the hydrogen electrosorption, and the peaks are most likely related to the HER.

Figures 8G–I show results obtained for the cell with MoS_2. Opposite to the carbon-based materials, the cell with MoS_2 exhibited higher capacitance values (ca. 150 Fg^{-1}) and higher intrinsic resistance, seen at each step of the voltage extension. It can be observed that the positive electrode operates with a wider potential window than the negative one. It may be explained by the possible redox reactions occurring on the negative electrode involving hydrogen ion, for example, ($MoS_2 + H^+ + e^- \rightarrow$ MoS-SH^+) which further leads to its evolution (Soon and Loh, 2007; Ji et al., 2015; Cao et al., 2019). The additional charge flowing through the system is being balanced on the positive electrode. The system worked relatively stable up to 0.8 V, where the decomposition reactions started to occur. Further voltage extension resulted in peaks showing at both negative and positive sides. Those peaks can be attributed to hydrogen and oxygen evolution. Such phenomena could be understood in the situation where the positive and negative electrodes are working near the thermodynamic limit of O_2 and H_2 evolution. Additionally, from the characteristics of the negative electrode, it looks that the hydrogen storage does not take place, there is a lack of peak related to desorption of hydrogen. Generally, the layers of TMDs are composed of inert basal plane and edge sites which remain electrochemically active (Gao et al., 2016). Therefore, dependent on the number of active sites exposed, the layered MoS_2 will promote hydrogen decomposition definitely excluding its electrosorption (Hinnemann et al., 2005; Soon and Loh, 2007; Ji et al., 2015; Shi et al., 2015; Voiry et al., 2016; Cao et al., 2019). It is visible on the CV of the negative electrode that the hydrogen sorption/desorption is not observed. **Figures 9A–F** show CV for both electrodes and separate positive and negative electrode performance of BP2000/MoS_2 and NTs/MoS_2 composites.

Cell working with BP2000/MoS_2 started to exhibit faradaic reaction above 1V, which is relatively higher if we compare it with the cell containing MoS_2. Additionally, peaks which can be attributed to the HER and OER are significantly smaller than those for MoS_2 sample. It can be explained by the synergetic effect of capacitive behavior of BP2000 and faradaic processes of the deposited MoS_2. It can be interpreted that the BP2000 could be responsible for the hydrogen storage and MoS_2 for the hydrogen evolution. Despite of only 7 wt% of the carbon in the full composite, these processes can be distinguished. The cell showed comparable shifts of the rest potential during voltage extension which is comparable to the cell with pure MoS_2. On the contrary, cell with NTs/MoS_2 showed significantly higher hydrogen evolution peaks than BP2000/MoS_2 and MoS_2. Carbon nanotubes are mainly mesoporous materials which cannot store hydrogen; on the other hand, they are structurally defected that promotes electrolyte decomposition. Additional peaks on the positive electrode which occurred during extension of voltage prove it. As the final effect, the composite based on nanotubes has demonstrated a smaller operational voltage window. Positive electrodes of both composites exhibit small humps during charging/discharging near 0.3–0.5 V. It should be stressed that MoS_2 exhibits the typical electrical double layer even if the specific surface area is low (40 m^2g^{-1}) but also redox reactions connected with Li^+ insertion accordingly:

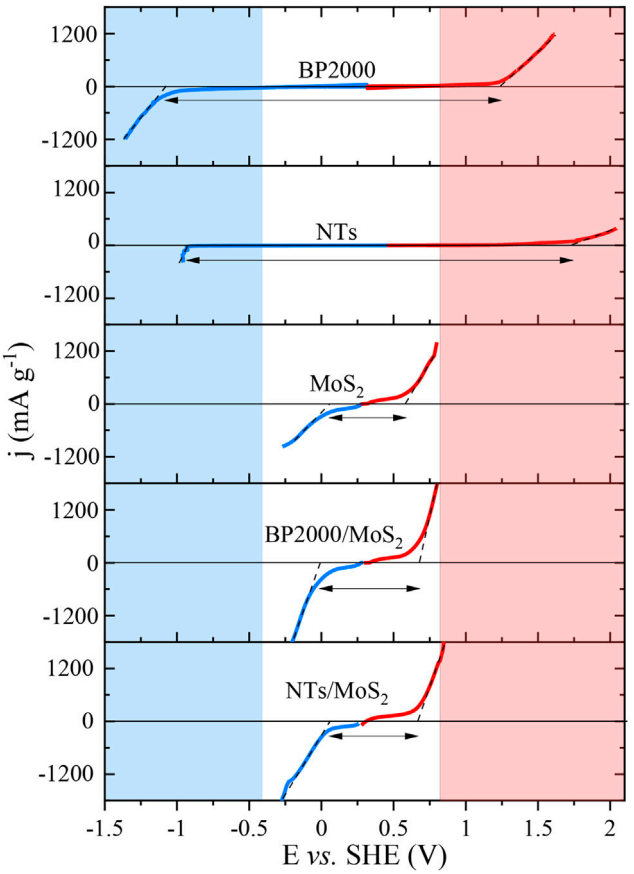

FIGURE 10 | Linear sweep voltammetry plots for different samples (pure materials and carbon/MoS_2 composites) at 2 mVs^{-1}.

$$MoS_2 + Li^+ + e^- \leftrightarrow MoS - SLi.$$

Redox reactions connected with the higher oxidation state of molybdenum should not be excluded.

Electrochemical stability of the electrodes working in a symmetrical two-electrode cell with reference was also determined with the use of linear sweep voltammetry (LSV). Voltage of the cell was extended from 0 to ± 1.5 V with a scan rate of 2 mVs^{-1} with simultaneous monitoring of electrodes potentials (Slesinski and Frackowiak, 2018). It was possible to observe real responses of each electrode since their performance are mutually governed. These investigations were conducted in two-electrode Swagelok cell with limited amount of electrolyte. This means that the local changes of the pH at electrode/electrolyte interface influence the electrodes behavior during voltage extension. The maximum operating window for each sample was determined by observing current increase related to hydrogen and oxygen evolution. The stability of each material with distinct electrodes is compiled in **Figure 10**. It can be marked that the BP2000 has the widest operational window. Thus, the potential was gradually extended in both directions, which is also reflected on CVs in **Figure 8**. LSV for NTs is characterized with narrower voltage window. In comparison to BP2000, hydrogen evolution on NTs occurs quicker, mostly due to the presence of defects and catalytic impurities, that is, Ni used for nanotubes production. MoS_2 in comparison to the carbon material showed much narrower voltage range of 0.6 V which is not a surprise due to its catalytic properties. What can also be observed is earlier evolution of hydrogen than in comparison with oxygen. Both composites, BP2000/MoS_2 and NTs/MoS_2, possess comparable HER and OER potentials. It can be also noticed that the composites possess slightly sharper anodic and cathodic responses. Such phenomena can be explained by significantly higher amount of vertically placed few-layered structures with exposed active edge sites which catalyze hydrogen and oxygen evolution reactions. Also, due to increased conductivity of the composites, the reaction of electrolyte decomposition can also occur earlier due to higher electron mobility.

CONCLUSION

Two morphologically different MoS_2 composites based on carbon nanotubes and carbon black have been prepared by a facile hydrothermal L-cysteine–assisted synthesis. Physicochemical characterization such as XRD and Raman spectroscopy proved that the desired materials were obtained. SEM/EDS and TEM analysis showed that the carbon supports are homogenously covered by the MoS_2 nanolayers. After physicochemical characterization, composites were prepared in a form of electrodes and their electrochemical performances in ECs cells were evaluated. NTs/MoS_2 and BP2000/MoS_2 demonstrated higher capacitance and intermediate conductivity to the parental materials—150 and 110 Fg^{-1} at 0.2 A g^{-1}, accordingly. MoS_2 was the major material in each composite; hence, main electrochemical responses were coming from the nanolayered structure of the TMD. Carbons served mainly as structural supports. Additional tests of the symmetric two-electrode cell with reference were performed. Investigation revealed that materials based on MoS_2 possess narrow range of operational voltage. On the contrary, carbon materials exhibited much wider operational voltage window. It was proven that MoS_2-based materials possess many active site edges which catalyze hydrogen evolution and restrict the operational voltage window to < 1 V. Additional experiments using the LSV method proved that pure MoS_2 possessed the narrowest voltage window of 0.6 V due to early hydrogen and oxygen evolution. BP2000/MoS_2 and NTs/MoS_2 composites exhibited comparable voltage range to MoS_2 but with slightly sharper anodic and cathodic responses caused by a vertical placement of few-layered structures with exposed active sites which catalyze HER and OER.

DATA AVAILABILITY STATEMENT

The original contributions presented in the study are included in the article/**Supplementary Material**, and further inquiries can be directed to the corresponding author.

AUTHOR CONTRIBUTIONS

EF contributed to research supervision, manuscript preparation, and results interpretation. MT contributed to planning and performing laboratory experiments and results interpretation. SS contributed to materials synthesis and manuscript preparation.

ACKNOWLEDGMENTS

The authors would like to acknowledge OPUS project of the National Science Center, Poland (Project No. 2018/31/B/ST4/01852) for the financial support of the research. The Polish Ministry of Science and Higher Education is also acknowledged for the 0911/SBAD/0399 project. The authors are sincerely thankful for performing TEM analysis to prof. Mirosława Pawlyta from Silesian University of Technology.

SUPPLEMENTARY MATERIAL

The Supplementary Material for this article can be found online at: https://www.frontiersin.org/articles/10.3389/fenrg.2021.647878/full#supplementary-material

REFERENCES

Acerce, M., Voiry, D., and Chhowalla, M. (2015). Metallic 1T Phase MoS2 Nanosheets as Supercapacitor Electrode Materials. *Nat. Nanotech.* 10, 313–318. doi:10.1038/nnano.2015.40

Balasingam, S. K., Lee, J. S., and Jun, Y. (2015). Few-layered MoSe2 Nanosheets as an Advanced Electrode Material for Supercapacitors. *Dalton Trans.* 44, 15491–15498. doi:10.1039/c5dt01985k

Bissett, M. A., Worrall, S. D., Kinloch, I. A., and Dryfe, R. A. W. (2016). Comparison of Two-Dimensional Transition Metal Dichalcogenides for Electrochemical Supercapacitors. *Electrochimica Acta* 201, 30–37. doi:10.1016/j.electacta.2016.03.190

Tseng, C.-A., and Lee, C.-P. (2020). Transition Metal Chalcogenides for the Electrocatalysis of Water. *Adv. Funct. Mater.* 19, 114. doi:10.5772/intechopen.92045

Cao, L., Yang, S., Gao, W., Liu, Z., Gong, Y., Ma, L., et al. (2019). Direct Laser-Patterned Micro-supercapacitors from Paintable MoS_2 Films. *Small* 9, 2905–2910. doi:10.1002/smll.201203164

Chang, K., and Chen, W. (2011). l-Cysteine-Assisted Synthesis of Layered MoS2/Graphene Composites with Excellent Electrochemical Performances for Lithium Ion Batteries. *ACS Nano* 5, 4720–4728. doi:10.1021/nn200659w

Chen, G. Z. (2016). Supercapacitor and Supercapattery as Emerging Electrochemical Energy Stores. *Int. Mater. Rev.* 62, 173–202. doi:10.1080/09506608.2016.1240914

Chen, W., Yu, X., Zhao, Z., Ji, S., and Feng, L. (2019). Hierarchical Architecture of Coupling Graphene and 2D WS2 for High-Performance Supercapacitor. *Electrochim. Acta* 298, 313–320. doi:10.1016/j.electacta.2018.12.096

Cherusseri, J., Sharma, R., and Kar, K. K. (2016). Helically Coiled Carbon Nanotube Electrodes for Flexible Supercapacitors. *Carbon* 105, 113–125. doi:10.1016/j.carbon.2016.04.019

Choi, W., Choudhary, N., Han, G. H., Park, J., Akinwande, D., and Lee, Y. H. (2017). Recent Development of Two-Dimensional Transition Metal Dichalcogenides and Their Applications. *Mater. Today* 20, 116–130. doi:10.1016/j.mattod.2016.10.002

Conley, H. J., Wang, B., Ziegler, J. I., Haglund, R. F., Pantelides, S. T., and Bolotin, K. I. (2013). Bandgap Engineering of Strained Monolayer and Bilayer MoS2. *Nano Lett.* 13, 3626–3630. doi:10.1021/nl4014748

Coogan, Á., and Gun'ko, Y. K. (2021). Solution-based "Bottom-Up" Synthesis of Group VI Transition Metal Dichalcogenides and Their Applications. *Mater. Adv.* 2, 146–164. doi:10.1039/d0ma00697a

Duesberg, G. S., Loa, I., Burghard, M., Syassen, K., and Roth, S. (2000). Polarized Raman Spectroscopy on Isolated Single-Wall Carbon Nanotubes. *Phys. Rev. Lett.* 85, 5436–5439. doi:10.1103/physrevlett.85.5436

Fic, K., Frackowiak, E., and Béguin, F. (2012). Unusual Energy Enhancement in Carbon-Based Electrochemical Capacitors. *J. Mater. Chem.* 22, 24213–24223. doi:10.1039/c2jm35711a

Frackowiak, E., and Béguin, F. (2001). Carbon Materials for the Electrochemical Storage of Energy in Capacitors. *Carbon* 39, 937–950. doi:10.1016/s0008-6223(00)00183-4

Gao, J., Li, L., Tan, J., Sun, H., Li, B., Idrobo, J. C., et al. (2016). Vertically Oriented Arrays of ReS2 Nanosheets for Electrochemical Energy Storage and Electrocatalysis. *Nano Lett.* 16, 3780–3787. doi:10.1021/acs.nanolett.6b01180

González, A., Goikolea, E., Barrena, J. A., and Mysyk, R. (2016). Review on Supercapacitors: Technologies and Materials. *Renew. Sustain. Energ. Rev.* 58, 1189–1206. doi:10.1016/j.rser.2015.12.249

Hinnemann, B., Moses, P. G., Bonde, J., Jorgensen, K. P., Nielsen, J. H., Horch, S., et al. (2005). Biomimetic Hydrogen Evolution: MoS_2 Nanoparticles as Catalyst for Hydrogen Evolution. *J. Am. Chem. Soc.* 127, 5208–5209. doi:10.1021/ja0504690

Huang, K.-J., Wang, L., Liu, Y.-J., Liu, Y.-M., Wang, H.-B., Gan, T., et al. (2013). Layered MoS2-Graphene Composites for Supercapacitor Applications with Enhanced Capacitive Performance. *Int. J. Hydrogen Energ.* 38, 14027–14034. doi:10.1016/j.ijhydene.2013.08.112

Huang, K.-J., Wang, L., Zhang, J.-Z., Wang, L.-L., and Mo, Y.-P. (2014). One-step Preparation of Layered Molybdenum Disulfide/multi-Walled Carbon Nanotube Composites for Enhanced Performance Supercapacitor. *Energy* 67, 234–240. doi:10.1016/j.energy.2013.12.051

Ji, H., Liu, C., Wang, T., Chen, J., Mao, Z., Zhao, J., et al. (2015). Porous Hybrid Composites of Few-Layer MoS2 Nanosheets Embedded in a Carbon Matrix with an Excellent Supercapacitor Electrode Performance. *Small* 11, 6480–6490. doi:10.1002/smll.201502355

Laheäär, A., Przygocki, P., Abbas, Q., and Béguin, F. (2015). Appropriate Methods for Evaluating the Efficiency and Capacitive Behavior of Different Types of Supercapacitors. *Electrochem. Commun.* 60, 21–25. doi:10.1016/j.elecom.2015.07.022

Lin, L., Lei, W., Zhang, S., Liu, Y., Wallace, G. G., and Chen, J. (2019). Two-dimensional Transition Metal Dichalcogenides in Supercapacitors and Secondary Batteries. *Energ. Storage Mater.* 19, 408–423. doi:10.1016/j.ensm.2019.02.023

Lukatskaya, M. R., Dunn, B., and Gogotsi, Y. (2016). Multidimensional materials and device architectures for future hybrid energy storage. *Nat. Commun.* 7, 12647. doi:10.1038/ncomms12647

Nasir, M. Z. M., Sofer, Z., Ambrosi, A., and Pumera, M. (2015). A Limited Anodic and Cathodic Potential Window of MoS2: Limitations in Electrochemical Applications. *Nanoscale* 7, 3126–3129. doi:10.1039/c4nr06899h

Pandolfo, A. G., and Hollenkamp, A. F. (2006). Carbon Properties and Their Role in Supercapacitors. *J. Power Sourc.* 157, 11–27. doi:10.1016/j.jpowsour.2006.02.065

Park, S.-K., Yu, S.-H., Woo, S., Quan, B., Lee, D.-C., Kim, M. K., et al. (2013). A Simplel-Cysteine-Assisted Method for the Growth of MoS2nanosheets on Carbon Nanotubes for High-Performance Lithium Ion Batteries. *Dalton Trans.* 42, 2399–2405. doi:10.1039/c2dt32137h

Rao, A. M., Ritcher, E., Bandow, S., Chase, B., Eklund, P. C., Williams, K. A., et al. (1997). Diameter-Selective Raman Scattering from Vibrational Modes in Carbon Nanotubes. *Science* 275, 187–191. doi:10.1126/science.275.5297.187

Ratajczak, P., Suss, M. E., Kaasik, F., and Béguin, F. (2019). Carbon Electrodes for Capacitive Technologies. *Energ. Storage Mater.* 16, 126–145. doi:10.1016/j.ensm.2018.04.031

Rendón-Patiño, A., Domenech-Carbó, A., Primo, A., and García, H. (2020). Superior Electrocatalytic Activity of MoS2-Graphene as Superlattice. *Nanomaterials* 10, 839. doi:10.3390/nano10050839

Sangeetha, D. N., and Selvakumar, M. (2018). Active-defective Activated carbon/MoS2 Composites for Supercapacitor and Hydrogen Evolution Reactions. *Appl. Surf. Sci.* 453, 132–140. doi:10.1016/j.apsusc.2018.05.033

Sangeetha, D. N., Santosh, M. S., and Selvakumar, M. (2020). Flower-like Carbon Doped MoS_2/Activated Carbon Composite Electrode for Superior Performance of Supercapacitors and Hydrogen Evolution Reactions, *J. Alloys Comp.* 831, 154745.

Sharma, P., and Bhatti, T. S. (2010). A Review on Electrochemical Double-Layer Capacitors. *Energ. Convers. Manage.* 51, 2901–2912. doi:10.1016/j.enconman.2010.06.031

Shi, S., Gao, D., Xia, B., Liu, P., and Xue, D. (2015). Enhanced Hydrogen Evolution Catalysis in MoS2 Nanosheets by Incorporation of a Metal Phase. *J. Mater. Chem. A.* 3, 24414–24421. doi:10.1039/c5ta08520a

Simon, P., and Gogotsi, Y. (2008). Materials for Electrochemical Capacitors. *Nat. Mater* 7, 845–854. doi:10.1038/nmat2297

Slesinski, A., and Frackowiak, E. (2018). Determination of Accurate Electrode Contribution during Voltammetry Scan of Electrochemical Capacitors. *J. Solid State. Electrochem.* 22, 2135–2139. doi:10.1007/s10008-018-3924-0

Soon, J. M., and Loh, K. P. (2007). Electrochemical Double-Layer Capacitance of MoS[sub 2] Nanowall Films. *Electrochem. Solid-state Lett.* 10, A250–A254. doi:10.1149/1.2778851

Sun, P., Wang, R., Wang, Q., Wang, H., and Wang, X. (2019). Uniform MoS2 Nanolayer with Sulfur Vacancy on Carbon Nanotube Networks as Binder-free Electrodes for Asymmetrical Supercapacitor. *Appl. Surf. Sci.* 475, 793–802. doi:10.1016/j.apsusc.2019.01.007

Voiry, D., Yang, J., and Chhowalla, M. (2016). Recent Strategies for Improving the Catalytic Activity of 2D TMD Nanosheets toward the Hydrogen Evolution Reaction. *Adv. Mater.* 28, 6197–6206. doi:10.1002/adma.201505597

Xu, D., Wang, H., Qiu, R., Wang, Q., Mao, Z., Jiang, Y., et al. (2020). Coupling of Bowl-like VS2 Nanosheet Arrays and Carbon Nanofiber Enables Ultrafast Na+-Storage and Robust Flexibility for Sodium-Ion Hybrid Capacitors. *Energ. Storage Mater.* 28, 91–100. doi:10.1016/j.ensm.2020.03.002

Yang, W., He, L., Tian, X., Yan, M., Yuan, H., Liao, X., et al. (2017). Carbon-MEMS-Based Alternating Stacked MoS2@rGO-CNT Micro-Supercapacitor with High 393 Capacitance and Energy Density. *Small* 13, 17000639. doi:10.1002/smll.201770144

Yuan, S., Pang, S. Y., and Hao, J. (2020). 2D Transition Metal Dichalcogenides, Carbides, Nitrides, and Their Applications in Supercapacitors and Electrocatalytic Hydrogen Evolution Reaction. *Appl. Phys. Rev.* 7–021304. doi:10.1063/5.0005141

Zdrojek, M., Gebicki, W., Jastrzebski, C., Melin, T., and Huczko, A. (2004). Studies of Multiwall Carbon Nanotubes Using Raman Spectroscopy and Atomic Force Microscopy. *Ssp* 99-100, 265–268. doi:10.4028/www.scientific.net/ssp.99-100.265

Zhang, W.-J., and Huang, K.-J. (2017). A Review of Recent Progress in Molybdenum Disulfide-Based Supercapacitors and Batteries. *Inorg. Chem. Front.* 4, 1602–1620. doi:10.1039/c7qi00515f

Zhong, C., Deng, Y., Hu, W., Qiao, J., Zhang, L., and Zhang, J. (2015). A Review of Electrolyte Materials and Compositions for Electrochemical Supercapacitors. *Chem. Soc. Rev.* 44, 7484–7539. doi:10.1039/c5cs00303b

Conflict of Interest: The authors declare that the research was conducted in the absence of any commercial or financial relationships that could be construed as a potential conflict of interest.